

MONOLITHIC 2GHZ ELECTROSTATICALLY ACTUATED MEMS OSCILLATOR WITH OPTO-MECHANICAL FREQUENCY MULTIPLIER

Siddharth Tallur, and Sunil A. Bhawe

OxideMEMS Lab, Cornell University, Ithaca, New York, USA

ABSTRACT

We present a silicon opto-acoustic oscillator operating at 2.05GHz with signal power +18dBm and phase noise -80dBc/Hz at 10kHz offset from carrier. We employ displacement amplification and partial air gap capacitive transduction to enhance the transduction efficiency. Built-in nonlinear opto-mechanical modulation provides noiseless upconversion of the oscillation signal all the way up to 16.4GHz with -45dBm signal power. We isolate oscillation harmonics at 4.1GHz and 6.15GHz and measure phase noise of -74dBc/Hz and -70dBc/Hz respectively at 10kHz offset from carrier. The monolithic opto-mechanical frequency multiplier eliminates the need for external active multipliers.

KEYWORDS

Opto-acoustic oscillator, Phase noise, Partial air gap transduction, Displacement amplification, ALD

INTRODUCTION

High Frequency Low Phase Noise MEMS Oscillators

Direct conversion radio architectures require oscillators operating at GHz rate frequencies with good phase noise performance. Oscillators based on electrostatically actuated MEMS resonators have been demonstrated in the few MHz-GHz frequency range [1,2,3]. At higher frequencies, the motional impedance of electrostatically transduced resonators is very large, and hence it is difficult to operate such a resonator in a feedback loop as an oscillator. Partial air gap transduction using atomic layer deposition (ALD) of various materials has been explored to reduce the motional impedance [4,5,6], but oscillators operating beyond 1GHz have not been reported. Piezoelectric transduction presents lower motional impedances at these frequencies, and piezoelectrically transduced Film Bulk Acoustic wave Resonator (FBAR) [7, 8, 9] and Contour Mode Resonator (CMR) [10, 11] based oscillators operating at few GHz frequencies have been demonstrated. Scaling these piezoelectric oscillators to even higher frequencies necessitates a thinner aluminum nitride film, which leads to mass-loading of the resonator due to the metal electrodes atop used to drive motion. This reduces the k_t^2 - Q (electromechanical coupling constant-quality factor product), which imposes practical limits on phase noise performance of oscillators with frequencies above 5GHz.

The Opto-Acoustic Oscillator (OAO)

In previous work, our group has demonstrated an opto-mechanical displacement scheme for electrostatically actuated MEMS resonators that utilizes the high displacement sensitivity of optical resonances to sense mechanical motion at frequencies all the way up to 9.8GHz [12]. This acousto-optic modulator has been

operated in a feedback loop to realize an opto-acoustic oscillator (OAO) and GHz rate mechanical oscillations using this transduction scheme have been achieved in the past [3]. However the device suffers from inefficient electrostatic transduction at frequencies beyond 1GHz [3, 12] and does not qualify as a candidate for designing a higher frequency oscillator.

This paper explores two innovations to the 2-coupled-ring resonator design to target a high frequency OAO. The first innovation is to use a micro-mechanical displacement amplifier [13] to achieve larger optical modulation [14]. The second innovation is to use partial air gap capacitive transduction to enhance the electromechanical transduction efficiency at higher frequencies. We incorporate both these ideas into the resonator design to demonstrate an electrostatically actuated silicon OAO operating at 2.05GHz. The oscillator has excellent phase noise of -80dBc/Hz at 10kHz offset from the carrier. The non-linearity of the optical sense scheme generates multiple oscillation harmonics all the way up to 16.4GHz. We isolate the second and third harmonics of the oscillation signal at 4.1GHz and 6.15GHz and measure phase noise of these oscillation signals to be -74dBc/Hz and -70dBc/Hz respectively at 10kHz offset from carrier.

DEVICE DESIGN AND FABRICATION

To achieve larger mechanical displacements and thus higher optical modulation, we employ the micromechanical displacement amplification scheme introduced by Li et al. [13]. We have earlier presented a silicon acousto-optic modulator employing this scheme [14] to achieve larger mechanical displacements at 1.09GHz.

To reduce the resonator-electrode gap, we transfer the released devices as fabricated in [14] into an ALD chamber and blanket coat the entire chip with 30nm alumina (Al_2O_3). We choose alumina as our ALD material due to its high dielectric constant (9.1). We then need to remove the alumina deposited on the bond pad to be able to make electrical contact to our device. Also we cannot spin coat photoresist on our sample as the released devices would then break off due to shear force. Instead we spray coat the sample with $6\mu\text{m}$ thick diluted photoresist (1:10 S1805:Acetone) and pattern the resist to expose the bond pads. We develop the resist using tetramethylammonium hydroxide (TMAH) based developer. This developer also simultaneously etches the exposed alumina without damaging the bond pads. We then strip the resist on the rest of the chip in acetone and finally dry the devices using a critical point dryer. Figure 1 shows an illustration of the fabrication process flow.

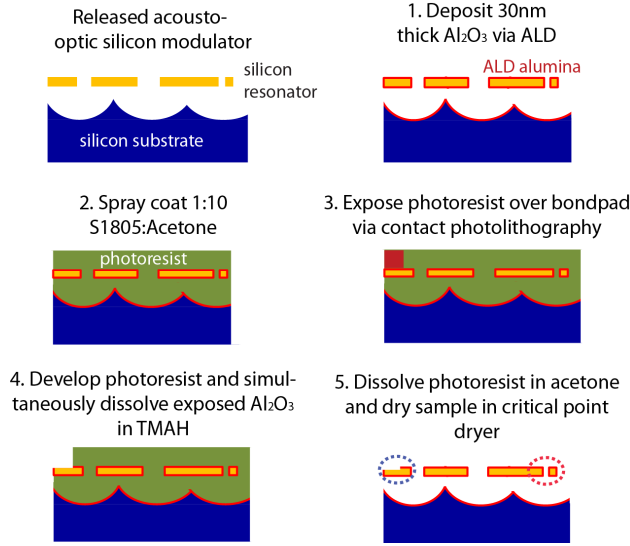


Figure 1: Process flow followed to fabricate a partial air gap transduced silicon acousto-optic modulator.

We start with a lithographically defined electrode-resonator gap of 130nm in silicon. This is reduced to 70nm post ALD. Figure 2 shows an SEM of the device highlighting the reduced gap.

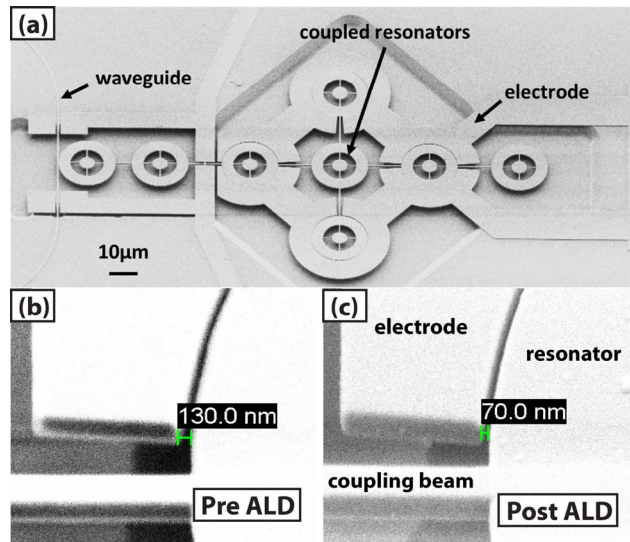


Figure 2: (a) Scanning electron micrograph (SEM) of the displacement amplifier based partial air gap capacitively transduced silicon acousto-optic modulator. The resonator-electrode gap is reduced from (b) 130nm prior to ALD to (c) 70nm post ALD.

EXPERIMENTAL MEASUREMENTS

Modulator characterization

We measure the optical response of the modulator prior to and post ALD. Light from a tunable diode laser is coupled into the on-chip waveguide through grating couplers and the transmitted power is measured using an optical power meter. Figure 3 shows the enhanced optical performance for the modulator post ALD. The grating transmission is boosted by 3dB, and the half-width-at-half-maximum bandwidth of the gratings increases from 15nm to 20nm.

We replace the optical power meter with a high bandwidth photoreceiver (Newfocus 1544-A) and use a

network analyzer to study the electromechanical transmission spectrum of the modulator. The laser wavelength is set 3-dB off resonance for a high optical Q (70,000) resonance at 1561nm. The ALD step does not lower the optical Q.

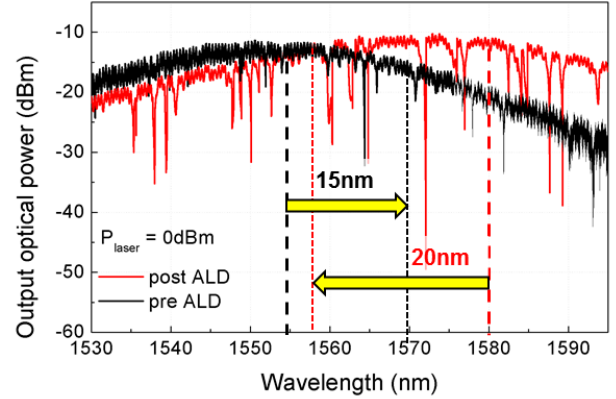


Figure 3: Optical transmission spectrum highlighting increase in grating transmission and bandwidth post ALD. The half-width-at-half-maximum bandwidth for the grating couplers increases from 15nm to 20nm.

Figure 4 shows the measured transmission response which shows a clear enhancement of signal strength for higher frequency modes, with the most notable improvement in insertion loss of 47dB at 2.05GHz. Mass loading of the resonator and the coupling beams due to ALD results in degradation of the mechanical Q from 2,300 prior to ALD to 1,098 post ALD, similar to that observed by Akgul et al. [5].

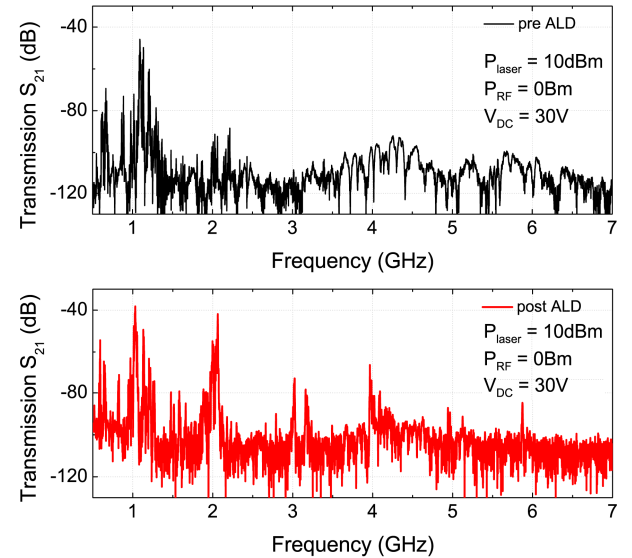


Figure 4: Comparison of the modulator transmission spectrum pre (top panel) and post (bottom panel) ALD. The most pronounced transduction enhancement is recorded at 2.05GHz (47dB improvement).

To select the second order compound radial expansion mode at 2.05GHz and suppress the other mechanical modes of the device, we use a band-pass filter (Mini-circuits VBFZ-2000-S+). Figure 5 shows the RF transmission spectrum measured by introducing the filter at frequencies near 2.05GHz. The spectrum shows 8

prominent peaks that arise from the 8-fold symmetry of the mutually coupled rings in the device vibrating in the second order compound radial expansion mode (Figure 5 inset). The other spurious peaks are attributed to imperfections in the beam lengths due to fabrication variations. The tallest peak at 2.047GHz corresponds to the mechanical mode with best momentum balance. The second tallest peak at 2.067GHz has a frequency separation of 20MHz from this mode and has 8dB larger insertion loss. Since the oscillator loop locks to a single mechanical mode, an oscillator operating at 2.047GHz will not be affected by the other mechanical modes.

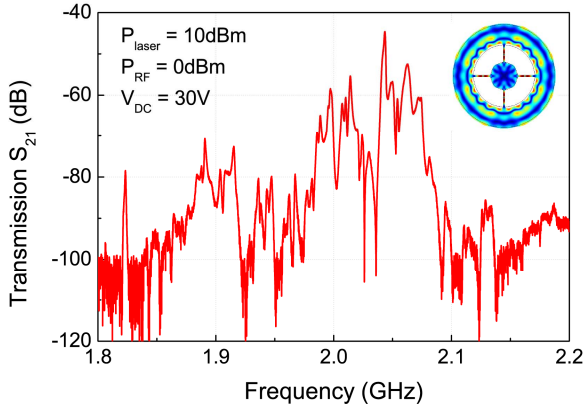


Figure 5: Transmission spectrum of the device measured with the introduction of a band-pass filter to select mechanical modes around 2GHz. Inset: Finite Element Method (FEM) simulated mechanical resonance mode shape at 2.047GHz.

2.05GHz Opto-Acoustic Oscillator

We operate the 2.05GHz mechanical resonance in a feedback loop using an amplifier (Mini-circuits ZQL-2700MLNW+) and a phase shifter using the oscillator topology outlined in [3]. Figure 6 below shows a schematic of the oscillator feedback loop.

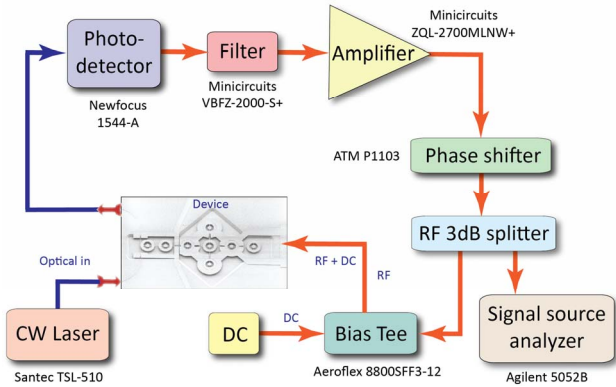


Figure 6: Schematic of the 2.05GHz oscillator loop.

Figure 7 shows the RF spectrum and phase noise of the oscillations at 2.05GHz. The oscillation signal phase noise at 10kHz offset from carrier is -80dBc/Hz . We measure the phase noise using an Agilent 5052B signal source analyzer. Using a low noise amplifier results in lack of $1/f^3$ slopes down to 5kHz offset from carrier in the phase noise plot unlike [3]. The $1/f^2$ corner frequency is observed to be $\approx 2\text{MHz}$, which is consistent with the

measured mechanical Q of 1,098.

Oscillation Harmonics

The mechanical motion of the ring resonator interrogated optically leads to a shift in its optical resonance frequency, and hence leads to modulation of the light coupled to the resonator. The optical resonance shape is Lorentzian, and therefore the modulation is non-linear. This results in generation of multiple harmonics of the fundamental oscillation frequency, as observed earlier in opto-mechanical oscillators which function based on the same modulation scheme [15, 16]. Figure 8 shows measured harmonics all the way up to 16.4GHz.

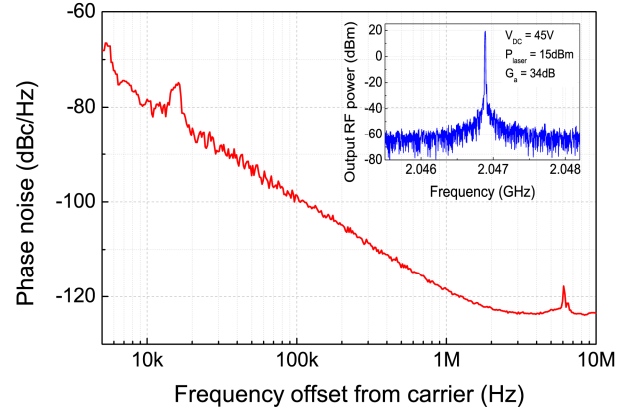


Figure 7: Phase noise of the oscillations at 2.05GHz, with -80dBc/Hz noise at 10kHz offset from carrier. Inset: RF spectrum of oscillations at 2.05GHz. The phase noise is measured using an Agilent 5052B signal source analyzer.

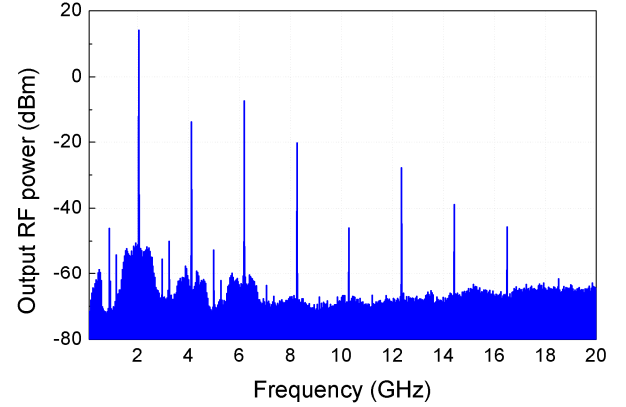


Figure 8: Plot showing various harmonics of the fundamental oscillations at 2.05GHz. The signal power at 16.4GHz is measured to be -45dBm .

Phase Noise of Higher Harmonics

We use band-pass filters to select the oscillation harmonics at 4.1GHz (VBFZ-4000+) and 6.15GHz (VBFZ-6260+) and measure their phase noise. The signals at these frequencies are expected to have the same noise signature as the fundamental harmonic at 2.05GHz. The non-linear shape of the optical resonance serves as an ideal frequency multiplier in this case, and hence the noise of all the higher oscillation harmonics of order n are expected to be worse than the phase noise of the 2.05GHz signal by $20\log(n)\text{dB}$. The phase noise at 4.1GHz and 6.15GHz signals follows this trend as seen in Figure 9.

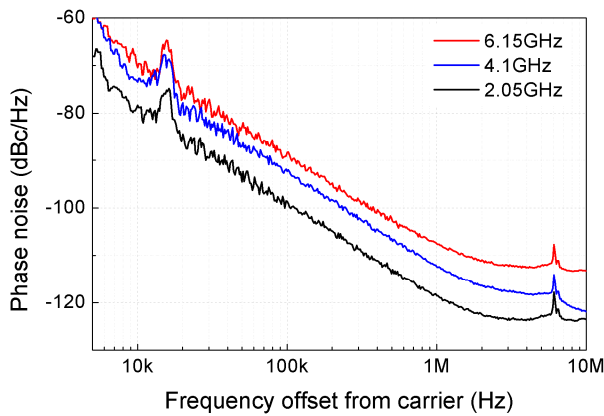


Figure 9: Comparison of phase noise of the oscillations at 2.05GHz, 4.1GHz and 6.15GHz. The phase noise for the higher harmonics of order n is worse than the fundamental by $20\log(n)$ dB. The RF oscillation signal power is the same for all curves (-5dBm).

Figure 10 shows RF spectrum of the oscillation harmonics at 10.3GHz and 12.35GHz. Due to unavailability of band-pass filters for these frequencies, the phase noise of these harmonics could not be measured.

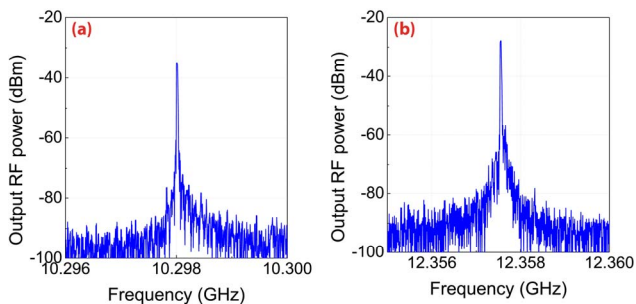


Figure 10: RF spectra of oscillations at (a) 10.3GHz and (b) 12.35GHz.

CONCLUSION

A combination of partial air gap capacitive transduction and micromechanical displacement amplification was employed to realize oscillations in a silicon MEMS resonator at 2.05GHz with RF power of 18dbm and phase noise of -80dBc/Hz at 10kHz offset from carrier. The device also benefits from the built-in opto-mechanical frequency multiplier, which yields high power harmonics of the oscillation signal all the way up to -45dBm signal power at 16.4GHz. The optical modulation serves as an ideal frequency multiplier, and the phase noise in the harmonics at 4.1 GHz and 6.15GHz are measured to be 6dB and 10dB worse than the noise at 2.05GHz as expected. The phase noise of these tones does not show any degradation due to the absence of an external mixer. These results constitute MEMS based frequency sources in the microwave X-band.

ACKNOWLEDGEMENTS

We express our thanks to Dr. Shantanu Rajwade and Laura Fegely of Cornell University, and Noah Clay at Cornell NanoScale Science and Technology Facility (CNF) for invaluable suggestions to design the process

flow. This work was funded by DARPA/MTO's ORCHID program and the devices were fabricated at CNF.

REFERENCES

- [1] G. K. Ho, F. Ayazi et al., "Temperature Compensated IBAR Reference Oscillators," *IEEE MEMS 2006, Istanbul*, pp. 910 - 913, 2006.
- [2] Y.-W. Lin, C. T.-C. Nguyen et al., "Low phase noise array-composite micromechanical wine-glass disk oscillator," *IEDM, Washington, DC*, pp. 218, 2005.
- [3] S. Sridaran et al., "1.12 GHz opto-acoustic oscillator," *MEMS 2012, Paris*, pp. 644-647, 2012.
- [4] L.-W. Hung, C. T.-C. Nguyen et al., "Capacitive Transducer Strengthening Via ALD-Enabled Partial-Gap Filling," *Hilton Head, SC*, pp. 208-211, 2008.
- [5] M. Akgul, C. T.-C. Nguyen et al., "Oscillator Far-From-Carrier Phase Noise Reduction Via Nano-Scale Gap Tuning of Micromechanical Resonators" *Transducers '09, Denver*, pp. 798-801, 2009.
- [6] S. Tallur et al., "Motional impedance analysis: bridging the 'gap' in dielectric transduction," *IEEE FCS 2011, San Francisco*, pp. 135-138, 2011.
- [7] B. P. Otis and J. M. Rabaey, "A 300- μ W 1.9-GHz CMOS oscillator utilizing micromachined resonators," *IEEE JSSC*, vol. 38, no. 7, pp. 1271-1274, 2003.
- [8] S. Rai, B. P. Otis et al., "A 1.5GHz CMOS/FBAR frequency reference with ± 10 ppm temperature stability," *IEEE EFTF-IFCS 2009, Besancon*, pp. 385-387, 2009.
- [9] R. Ruby et al., "Positioning FBAR technology in the frequency and timing domain," *IEEE TUFFC*, vol. 59, no. 3, pp. 334-345, 2012.
- [10] C. Zuo, G. Piazza et al., "1.05 GHz MEMS Oscillator Based On Lateral-Field-Excited Piezoelectric AlN Resonators," *IEEE EFTF-IFCS 2009, Besancon*, pp. 381-384, 2009.
- [11] C. Zuo, G. Piazza et al., "Switch-less dual-frequency reconfigurable CMOS oscillator using one single piezoelectric AlN MEMS resonator with co-existing S0 and S1 Lamb-wave modes," *IEEE MEMS 2011, Cancun*, pp. 177-180, 2011.
- [12] S. Tallur et al., "Comparison of f-Q scaling in wineglass and radial modes in ring resonators," *IEEE MEMS 2013, Taipei*, pp. 777-780, 2013.
- [13] Y. Lin, C. T.-C. Nguyen et al., "Digitally-specified micromechanical displacement amplifiers," *Transducers '09, Denver*, pp. 781-784, 2009.
- [14] S. Tallur et al., "Electro-mechanically induced GHz rate optical frequency modulation in silicon," *IEEE Photonics Jour.*, vol. 4, no. 5, pp. 1474-1483, 2012.
- [15] S. Tallur et al., "A monolithic radiation-pressure driven, low phase noise silicon nitride opto-mechanical oscillator," *Optics Express*, vol. 19, pp. 24522-24529, 2011.
- [16] T. Rocheleau, C. T.-C. Nguyen et al., "Enhancement of mechanical Q for low phase noise optomechanical oscillators," *MEMS 2013, Taipei*, pp. 118-121, 2013.

CONTACT

*S. Tallur, tel: +1-607-279-7818; sgt28@cornell.edu